Check for updates

Selective extracellular arginine deprivation by a single injection of cellular non-uptake arginine deiminase nanocapsules for sustained tumor inhibition†

Hongzhao Qi, [ID] *[a] Yin Wang,[a] Xubo Yuan, [ID] [c] Peifeng Li[a] and Lijun Yang [ID] *[b]

The metabolic enzyme-based arginine deprivation represents a tremendous opportunity to treat argininosuccinate synthetase (ASS1)-deficient tumors. Arginine deiminase (ADI), a typical representative, has aroused great interest. To date, the functional modification of ADI, such as PEGylation, has been applied to improve its weakness significantly, reducing its immunogenicity and extending its blood circulation time. However, the advantages of ADI, such as the cellular non-uptake property, are often deprived by current modification methods. The cellular non-uptake property of ADI only renders extracellular arginine degradation that negligibly influences normal cells. However, current-functionalized ADIs can be readily phagocytized by cells, causing the imbalance of intracellular amino acids and the consequent damage to normal cells. Therefore, it is necessary to exploit a new method that can simultaneously improve the weakness of ADI and maintain its advantage of cellular non-uptake. Here, we utilized a kind of phosphorylcholine (PC)-rich nanocapsule to load ADI. These nanocapsules possessed extremely weak cellular interaction and could avoid uptake by endothelial cells (HUVEC), immune cells (RAW 264.7), and tumor cells (H22), selectively depriving extracellular arginine. Besides, these nanocapsules increased the blood half-life time of ADI from the initial 2 h to 90 h and efficiently avoided its immune or inflammatory responses. After a single injection of ADI nanocapsules into H22 tumor-bearing mice, tumors were stably suppressed for 25 d without any detectable side effects. This new strategy first realizes the selective extracellular arginine deprivation for the treatment of ASS1-deficient tumors, potentially promoting the clinical translation of metabolic enzyme-based amino acid deprivation therapy. Furthermore, the research reminds us that the functionalization of drugs can not only improve its weakness but also maintain its advantages.

1. Introduction

Tumor metabolism, which is the target for treating certain malignancies, has recently triggered increased interest.[1] The depletion of amino acids that are necessary for tumor survival with metabolic enzymes is a typical representative and has been successfully used in clinical trials.[2] Arginine, originating from citrulline *via* the catalysis of argininosuccinate synthetase

(ASS1) and argininosuccinate lyase (ASL), is a kind of nonessential amino acid in adult humans.[3] Some malignant cells, however, must rely on exogenous arginine for their growth and proliferation due to lack of ASS1, which is the key rate-limiting enzyme in the synthesis of arginine.[4] Therefore, these kinds of tumors can be efficiently suppressed by the metabolizing enzyme-based degradation of arginine in the blood.[5] At present, human arginase-1 (Arg-1) and bacterial arginine deiminase (ADI) are the common enzymes that have been used for arginine deprivation.[6] Arg-1 can catalyze arginine into ornithine and urea, but it has a low affinity for arginine and a non-physiological optimum pH, severely hampering its use.[7,8] ADI, by contrast, can efficiently convert arginine into citrulline and ammonia, and the resulting citrulline can be recycled back to arginine in normal cells, avoiding potential side effects.[9] Furthermore, ADI is specific for arginine and does not degrade other amino acids.[10] Thus, ADI is an optimized enzyme for arginine deprivation therapy. However, its clinical

[a]*Institute of Translational Medicine, The Affiliated Hospital of Qingdao University, College of Medicine, Qingdao University, Qingdao 266021, China. E-mail: qihongzhao@qdu.edu.cn*
[b]*College of Materials Science and Engineering, Qingdao University of Science and Technology, Qingdao 266042, China. E-mail: lijunyang@qust.edu.cn*
[c]*Tianjin Key Laboratory of Composite and Functional Materials, School of Materials Science and Engineering, Tianjin University, Tianjin 300072, China*
†Electronic supplementary information (ESI) available. See DOI: 10.1039/d0nr06823c

application is still limited due to the high immunogenicity and short blood circulation time.

The functionalization of ADI has been applied to overcome its disadvantages. The PEGylation of ADI is the most widely used method, and its effectiveness has been evaluated in clinical trials.[11,12] PEGylation can extend the blood circulation time and reduce the immunogenicity of ADI. However, its activity is dramatically decreased because of the random chemical reaction between ADI and PEG. As an example, PEGylated ADI from mycoplasma only retains 50% of its original enzymatic activity.[10] Furthermore, although the hydration effect of PEG increases the hydrophilicity of ADI, the hydrophobic backbone and methoxy terminal of amphiphilic PEG still render immunogenicity.[13] The PEG-driven immune response can accelerate the clearance of PEGylated ADI, diminishing its therapeutic effects and even causing lethal side effects. Nanocarriers have been recently exploited to encapsulate ADI via non-covalent means, efficiently maintaining the activity of ADI. For example, carboxymethyl chitosan-based vesicles have been used as ADI nanoreactors for arginine deprivation, and the activity of the encapsulated ADI is nearly identical to that of native ADI.[14] The improvement of decoration methods, to date, appears to have efficiently overcome the shortages of ADI. However, the exploitation of these methods has always cast a shadow, which is never taken seriously, over the clinical translation of ADI.

Traditionally, it is believed that arginine deprivation through ADI is a nontoxic method to cells that can normally express ASS1, but this kind of situation is based on extracellular arginine deprivation since native ADI cannot directly enter cells.[15] On the contrary, the functional modifications change the interaction between ADI and cells and often result in its cellular uptake, increasing the ratio of intracellular citrulline to arginine and potentially damaging the normal cells. As an example, delivering ADI into tumor cells that highly express ASS1 efficiently inhibits their proliferation.[16] Therefore, the current decoration methods endow ADI with the cellular uptake property, resulting in the potential toxicity to normal cells and tissues. This mechanism can also explain why PEGylated ADI often causes adverse effects in clinical trials. Therefore, exploiting a new method to improve the weakness of ADI and maintain its advantage of cellular non-uptake could not only efficiently suppress ASS1-deficient tumors but also dramatically reduce side effects.

It has been proved that the translocation of nanocarriers into the cell starts from the adhesion of nanocarriers onto the surface of cells. Therefore, reducing the cellular adhesion of nanocarriers can potentially render them incapable for cellular uptake. Here, we constructed a kind of phosphorylcholine (PC)-containing ADI nanocapsule with weak cellular interaction (denoted as WIT-n(ADI)) by in situ polymerization on the ADI surface with 2-methacryloyloxyethyl phosphorylcholine (MPC) and N,N'-methylene bisacrylamide (BIS). As a control, ADI nanocapsules with strong cellular interaction (denoted as SIT-n(ADI)) were also synthesized using acrylamide (AAM) as a polymeric monomer. WIT-n(ADI), which was prepared with a

rational PC surface filling ratio (80%), possessed the characteristics of extremely weak cellular interaction, successfully avoiding the uptake of WIT-n(ADI) by endothelial cells, immune cells, and tumor cells. The circulating half-life time of WIT-n (ADI) was ~90 h, and even after 240 h, ~25% of WIT-n(ADI) can still be present in the blood. The super-long circulated WIT-n(ADI) can persistently catalyze arginine into citrulline, leading to the sustained high ratio of citrulline to arginine in plasma. Besides, the application of WIT-n(ADI) did not show any significant effect on the intracellular ratio of citrulline to arginine in normal cells because of the cellular non-uptake property of WIT-n(ADI). After a single-tail intravenous injection of WIT-n(ADI), subcutaneous H22 cell tumor models were continuously suppressed without detectable side effects. Furthermore, WIT-n(ADI) did not show detectable immune or inflammatory responses because the zwitterionic PC-containing polymers were entirely hydrophilic, possessing a minimal propensity for any hydrophobic interaction and exhibiting much lower immunogenicity than PEG.[17–19] This new strategy first realizes the selective extracellular arginine deprivation for the treatment of ASS1-deficient tumors, potentially promoting the clinical translation of metabolic enzyme-based amino acid deprivation therapy.

2. Materials and methods

2.1 Materials

All chemical reagents were of analytical reagent grade and purchased from Sigma unless otherwise indicated. ADI crude extract was purchased from Beijing Baiaolaibo Technology Co., Ltd. ELISA kits (IL-6, IL-10, TNF-α, and IFN-γ), bicinchoninic acid (BCA) protein assay kit, Sephadex G-100, and phenyl-sepharose CL-4B were obtained from Solarbio. ELISA kits (TP, AST, ALT, and ALP) were purchased from MSKBIO Technology Ltd. Cell counting kit-8 (CCK-8) was purchased from US Everbright Inc. Arginine assay kit and citrulline assay kit were purchased from BioVision Incorporated. Rhodamine B isothiocyanate and Cy5.5 NHS ester were purchased from Shanghai Yuanye Biological Technology Co., Ltd. Cell culture medium and serum were purchased from Guangzhou Jet Bio-Filtration Co., Ltd.

2.2 Synthesis and characteristics of WIT-n(ADI)

ADI crude extract was first purified by Sephadex G-100, and the purified ADI was quantified using a BCA protein assay kit. WIT-n(ADI) was synthesized by a method reported in our previous studies but with slight modifications.[20] ADI was pre-conjugated with acryloyl groups using N-hydroxysuccinimide esters. Then, the acrylated ADI solution was mixed with MPC and BIS, and polymerization was initiated by adding ammonium persulfate (APS) and N,N,N',N'-tetramethylethylenediamine (TEMED). Polymerization proceeded in a nitrogen atmosphere at 4 °C for 120 min. MPC was substituted by AAM to synthesize SIT-n(ADI) according to the above-mentioned process. The resulting nanocapsules were purified by

passing through a phenyl-sepharose CL-4B column and dialyzing against PBS.

The size and zeta potential of native ADI, SIT-n(ADI), and WIT-n(ADI) were measured by dynamic light scattering (DLS, BI-90Plus, Brookhaven Instruments Ltd, USA), and the samples were analyzed in triplicate. Their morphologies were assessed using a high-resolution transmission electron microscope (TEM, JEM-2100F, JEOL Ltd, Japan), and the samples were stained with 2% phosphotungstic acid before observation. The FT-IR spectrum analysis of lyophilized native ADI, SIT-n(ADI), and WIT-n(ADI) was performed with KBr pellets using an FTIR spectrometer (Nicolet IS10, Thermo Scientific, USA). Native ADI, SIT-n(ADI), and WIT-n(ADI) solutions (0.2 mg mL^{-1}) were also measured using a UV-vis spectrophotometer (T9, Puxi Instrument, China). Circular dichroism (CD) analysis was performed using a spectrophotometer (Model J-810, Jasco, Tokyo, Japan). Native ADI, SIT-n(ADI), and WIT-n(ADI) were prepared at a concentration of 0.2 mg mL^{-1}. Measurements were collected over the wavelength range of 250–190 nm.

2.3 Specific activity test of WIT-n(ADI)

The enzymatic activities of native ADI, SIT-n(ADI), and WIT-n(ADI) were assayed using an arginine assay kit. Briefly, 0.1 mg mL^{-1} of native ADI, SIT-n(ADI), and WIT-n(ADI) were respectively incubated with 50 mM arginine at 37 °C for 10 min. An arginine assay kit measured the concentrations of residual arginine. One unit of enzymatic activity was defined as the amount of enzyme that catalyzes 1.0 μmol of arginine into citrulline per minute under assay conditions. The specific activity is the ratio of enzymatic activity to protein concentration.

To test the stability of WIT-n(ADI), we incubated native ADI, SIT-n(ADI), and WIT-n(ADI) with mouse serum (volume ratio was 1 : 1) and stored at 4 °C and 37 °C respectively. Then, every five days, the enzymatic activities of native ADI, SIT-n(ADI), and WIT-n(ADI) were tested according to the above-mentioned method. The test continued for 60 days.

2.4 The hydrophilicity determination of WIT-n(ADI)

The static water contact angles of native ADI, SIT-n(ADI), and WIT-n(ADI) were measured using a Lauda Scientific surface analyzer LSA 60 at room temperature. Samples (1 mg mL^{-1}) were added dropwise onto the surface of a silicon wafer, respectively. Then, the solution was dried under N$_2$ flow to form a sample-coated silicon wafer. Finally, a drop of ultrapure water was placed on the surface of the silicon wafer using a microsyringe, and the static water contact angle was recorded.

2.5 The cellular uptake of WIT-n(ADI)

Human umbilical vein endothelial cells (HUVEC), hepatocarcinoma-22 (H22) cells, and RAW 264.7 cells were seeded on the glass coverslips (pretreated with polylysine) of a six-well plate at a density of 1×10^4 cells per well and cultured overnight at 37 °C respectively. Then, the cells were cultured for 24 h with fresh culture media in the presence of native ADI, SIT-n(ADI), and WIT-n(ADI) labeled with rhodamine B (200 ng mL^{-1}). After 24 h of incubation, the cells were washed twice with PBS and fixed with paraformaldehyde (4%) for 10 min. Following the wash with PBS, the cells were respectively labeled with FITC-phalloidin and DAPI and imaged using an Olympus IX81 microscope.

HUVEC cells, H22 cells, and RAW 264.7 cells were seeded in six-well plates at a density of 1×10^5 cells per well and then incubated with rhodamine B-labeled native ADI, SIT-n (ADI), and WIT-n(ADI) (200 ng mL^{-1}) for 24 h. Then, the cells were harvested, and fluorescence-activated cell sorting (FACS) was employed to count rhodamine B-positive cells. Finally, 10 000 cells were counted and analyzed by measuring the signal from the rhodamine B channel. Each test was repeated three times.

2.6 Cell viability assay

Cell suppression effects of native ADI, SIT-n(ADI), and WIT-n (ADI) were evaluated using a CCK-8 kit. First, HUVEC cells, H22 cells, and RAW 264.7 cells were seeded into 96-well plates at a density of 4000 cells per well and grown in a complete medium at 37 °C for 24 h. Subsequently, the culture medium was replaced with a complete medium containing different concentrations of native ADI, SIT-n(ADI), and WIT-n(ADI). At 48 h, a CCK solution was added, and the cell viability was assessed. Unexposed wells were regarded as the control, and the cell viability was calculated as the ratio of the absorbance (450 nm) of the test and control wells.

2.7 Test of the intracellular ratio of citrulline to arginine

HUVEC cells, H22 cells, and RAW 264.7 cells were respectively seeded in six-well plates and incubated overnight. The cells were then treated with different concentrations of native ADI, SIT-n(ADI), and WIT-n(ADI). After 24 h of incubation, the cells were washed with PBS and detached with trypsin. Distilled water was added to the detached cell pellets, which were subsequently rigorously vortexed and centrifuged at 14 000 rpm for 30 min. The supernatant was collected, and the concentrations of intracellular citrulline and arginine were measured using the corresponding assay kits.

2.8 Blood circulation of WIT-n(ADI)

To test the blood circulation time of WIT-n(ADI), healthy female Kunming mice were separated into three groups (native ADI, SIT-n(ADI), and WIT-n(ADI)) with 6 mice in each group. The solution of rhodamine B-labeled native ADI, SIT-n(ADI), and WIT-n(ADI) was single-dose injected *via* the tail vein. The equivalent ADI was ~1 mg. All experimental protocols were conducted following the guidelines for Animal Experimentation of the Affiliated Hospital of Qingdao University and approved by the Committee for Animal Experimentation. At selected time points, blood was collected and centrifuged to obtain plasma. The fluorescence intensity of the plasma was tested using a microplate reader.

2.9 Test of the ratio of citrulline to arginine in plasma and tumor tissues

Healthy female Kunming mice were separated into three groups (native ADI, SIT-n(ADI), and WIT-n(ADI)) with 6 mice in each group. Native ADI, SIT-n(ADI), and WIT-n(ADI) solution were respectively single-dose injected *via* the tail vein. The equivalent ADI was ~1 mg. At selected time points, blood was collected through the tail cut and separated for plasma. Corresponding assay kits were used to measure the concentrations of citrulline and arginine in plasma. Besides, tumor tissues were harvested at selected time points to extract citrulline and arginine. The concentration of citrulline and arginine in tumor tissues was measured using assay kits.

2.10 Immunogenicity evaluations by assessing inflammatory cytokine secretion

Healthy female Kunming mice were separated into four groups (control, native ADI, SIT-n(ADI), and WIT-n(ADI)) with 6 mice in each group. PBS, native ADI, SIT-n(ADI), and WIT-n(ADI) solutions were respectively single-dose injected *via* the tail vein. The equivalent ADI was ~1 mg. At selected time points, the blood samples were collected from the mice using a coagulant tube, which allows the blood to coagulate naturally, and then centrifuged at 2000 rpm for 10 min. The serum was collected, and corresponding ELISA kits were used to analyze the levels of IL-6, IL-10, TNF-α, and IFN-γ.

2.11 *In vivo* bio-distribution of WIT-n(ADI)

Healthy female nude mice were separated into three groups, with 6 mice in each group. The solution of Cy5.5-labeled native ADI, SIT-n(ADI), and WIT-n(ADI) were single-dose injected *via* the tail vein. The equivalent ADI was ~1 mg. After 24 h of intravenous injection, the bio-distributions of Cy5.5-labeled native ADI, SIT-n(ADI), and WIT-n(ADI) in nude mice were studied using an IVIS imaging system. After observation, mice were killed, and the heart, liver, spleen, lung, and kidney were harvested for the qualitative and quantitative determination of fluorescence intensity.

To further confirm the bio-distribution of WIT-n(ADI), healthy female nude mice were separated into three groups with 6 mice in each group and injected with Cy5.5-labeled native ADI, SIT-n(ADI), and WIT-n(ADI), respectively. After 24 h of intravenous injection, mice were anesthetized and cardiac perfused with PBS. After cardiac perfusion, the heart, liver, spleen, lung, and kidney of mice were taken for the qualitative and quantitative determination of fluorescence intensity.

2.12 *In vivo* antitumor efficiency of WIT-n(ADI)

ASS1-deficient H22 cells were chosen as the model cells. They were suspended in serum-free DMEM medium and were subcutaneously inoculated to the flank of the mice (5×10^6 cells per mice). Four days after tumor inoculation, the tumor-bearing mice were divided randomly into four groups (control, native ADI, SIT-n(ADI), and WIT-n(ADI)). Each group had eight mice. PBS and sample solutions were intravenously adminis-

tered only once, and the equivalent ADI was ~1 mg. Mice weight and their tumor length and width were measured every three days. Consistent with our previous research, the tumor volume was calculated according to the formula (volume = length × width^2/2).[21] The mice were euthanized, and the tumors were harvested. The tumors were photographed, and their average masses were measured. Immunohistochemistry (IHC) was performed for analyzing the expression levels of caspase-3 and Bcl-2. For the observation of tumor cell apoptosis, tumor slices were stained with hematoxylin and eosin (H&E) and terminal deoxynucleotidyl transferase (TdT)-mediated dUTP nick end labeling (TUNEL), respectively.

2.13 Biological safety of WIT-n(ADI)

After treatment, besides tumors, the heart, liver, spleen, lung, and kidney of mice were harvested to store overnight in 4.0% (v/v) paraformaldehyde solution in PBS. Then, they were washed twice with PBS to remove excess paraformaldehyde. Paraffin-embedded tissue sections were stained with H&E and observed through a microscope. Besides, the serum levels of total protein (TP), aspartate aminotransferase (AST), alanine aminotransferase (ALT), and alkaline phosphatase (ALP) were determined using the corresponding ELISA kits.

2.14 Statistical analysis

Statistical comparisons were achieved using a one-way ANOVA with a Dunnett *post hoc* test using the GraphPad Prism 7.0 software.

3. Results and discussion

3.1 Construction and characterization of WIT-n(ADI)

The preparation process of WIT-n(ADI) is shown in Scheme 1A. MPC and BIS were respectively used as the monomer and the non-degradable crosslinker. When the pH of the solution was adjusted to 6.5, MPC and BIS would aggregate around ADI because it was an acidic protein, relying on electrostatic interaction and hydrogen-bond interaction.[22] APS and TEMED triggered the polymerization of monomers and crosslinkers to encapsulate ADI *in situ*. As a control, ADI nanocapsules with strong cellular interaction (denoted as SIT-n(ADI)) were also synthesized using acrylamide (AAM) as a polymeric monomer, and the rest was consistent with the above description.

We have previously exploited a similar kind of nanocapsule for the extracellular delivery of protein drugs.[23] To endow these nanocapsules with the ability of extracellular enzyme-responsive degradation, we had to control the surface PC filling ratios at 50.5%–58.3%. This compromise choice came at the expense of the circulation time of nanocapsules. By comparison, WIT-n(ADI) did not need to be degraded because arginine could diffuse through the polymeric shell of WIT-n(ADI),[24] and thus the surface PC filling ratio of WIT-n(ADI) could be further increased. However, it was difficult to adjust the surface PC filling ratio of WIT-n(ADI) higher than 80%
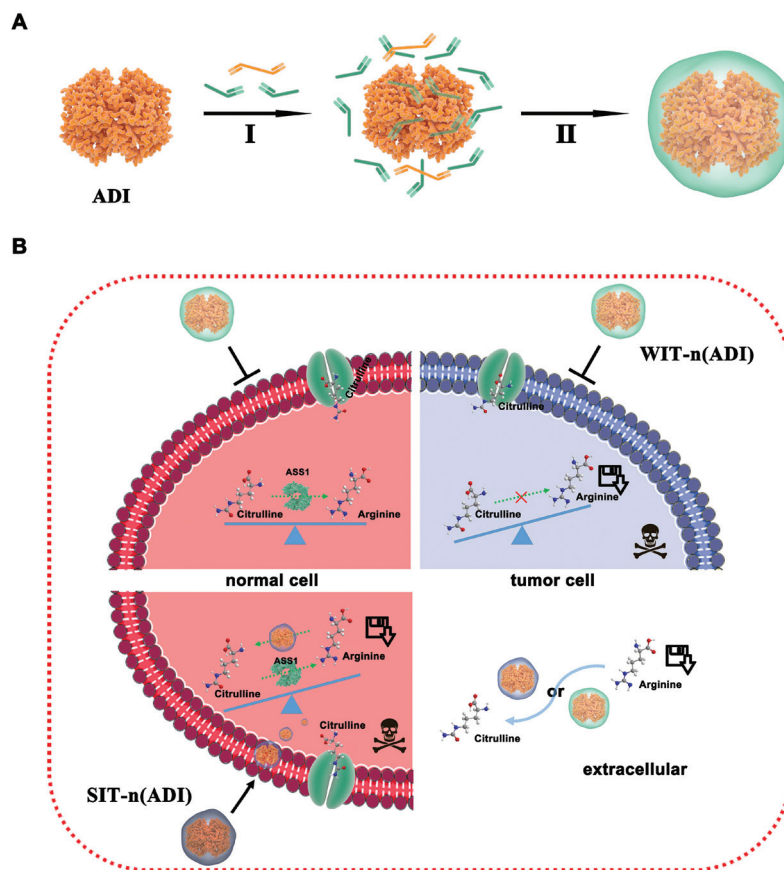
Scheme 1 Preparation and therapeutic mechanism of WIT-n(ADI). (A) Preparation of ADI nanocapsules. Step I: monomers and crosslinkers were enriched around individual ADI *via* electrostatic and hydrogen bond interactions; step II: free radical polymerization was initiated to form a thin polymeric shell around ADI. AAM and MPC were respectively used as monomers to prepare SIT-n(ADI) and WIT-n(ADI). (B) Therapeutic mechanism of WIT-n(ADI). WIT-n(ADI) could catalyze extracellular arginine into citrulline and indirectly reduce the intracellular arginine concentration of ASS1-deficient tumor cells, efficiently suppressing their growth. Furthermore, WIT-n(ADI) could not be taken up by normal cells, leading to their negligible influence on the intracellular arginine concentration and the undetectable side effects. In contrast, SIT-n(ADI) could be efficiently taken up by normal cells, resulting in the imbalance of intracellular arginine and citrulline and the consequent toxicity.

because excess monomers would readily result in the formation of the bulk hydrogel. Here, we increased the PC filling ratio of WIT-n(ADI) to ~80%, potentially endowing WIT-n(ADI) with super-hydrophilicity.

To verify the successful preparation, we characterized the synthetic products. The morphology of native ADI (Fig. S1†) was ruleless and exhibited a certain amount of aggregation potentially caused by heavy metal salt-based negative staining agents.[25] The representative TEM images of SIT-n(ADI) and WIT-n(ADI) (Fig. 1A and B) present that they were both spherical shapes and had good dispersion, implying the protection to ADI based on nanocapsules. Compared with SIT-n(ADI), WIT-n(ADI) is more uniform in size. Consistent with the TEM observation, the dynamic light scattering (DLS) measurement (Fig. 1C) showed that the diameter of WIT-n(ADI) was 27 ± 3 nm (PDI was ~0.112), while that of SIT-n(ADI) was 28 ± 10 nm (PDI was ~0.357). These results indicated that the mean diameter of SIT-n(ADI) was similar to that of WIT-n(ADI), but WIT-n(ADI) displayed better uniformity. This difference may be because of the unique hydration state of PMPC.[26] As a kind

of acidic protein, ADI has electronegativity with a mean zeta potential of −10.46 mV in the physiological state. In comparison, the mean zeta potential of SIT-n(ADI) and WIT-n(ADI) were both nearly 0 mV because of the shielding effect of the AAM or MPC-based electroneutral polymer shells (Fig. 1D). The surface neutral zeta potential of WIT-n(ADI) was beneficial to its great blood circulation since nanoparticles with too high or too low surface potential were readily cleared by the immune system.[27] Furthermore, the neutral zeta potential could dramatically reduce the interaction between WIT-n(ADI) and cells, avoiding its cellular uptake.

We further characterized the structure and components of WIT-n(ADI). The FT-IR spectrum of WIT-n(ADI) exhibited new peaks at 1710, 1240, 1090, and 970 cm^{-1} (Fig. 1E), which were the typical peaks of MPC-based polymer networks.[28] The spectrum new peaks of SIT-n(ADI) exhibited at 1617, 1560, 1350, and 1119 cm^{-1} indicate the formation of the AAM-based polymeric shell around ADI.[29] UV-vis spectra also proved the shielding effect of polymeric shells on ADI. Different from native ADI, SIT-n(ADI) and WIT-n(ADI) did not show the
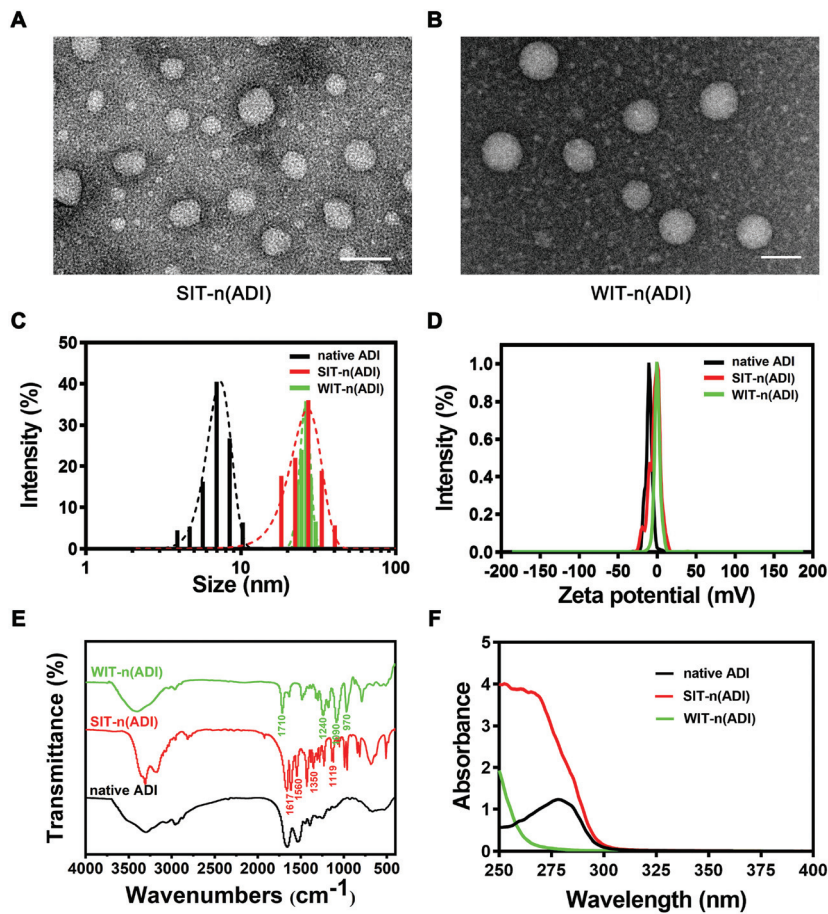
Fig. 1 Characterization of WIT-n(ADI). (A and B) Representative TEM images of SIT-n(ADI) and WIT-n(ADI). The scale bar was 50 nm. (C) Hydrodynamic size distribution of native ADI, SIT-n(ADI), and WIT-n(ADI). (D) Zeta potential of native ADI, SIT-n(ADI), and WIT-n(ADI) in PBS. (E) FT-IR spectra of native ADI, SIT-n(ADI), and WIT-n(ADI) after lyophilization. (F) UV-vis spectrum of native ADI, SIT-n(ADI), and WIT-n(ADI).

characteristic absorption peak of proteins at 280 nm (Fig. 1F). We further identified the ADI core of SIT-n(ADI) and WIT-n(ADI) by circular dichroism (CD) analysis (Fig. S2†). In conclusion, these results indicated the successful preparation of ADI nanocapsules.
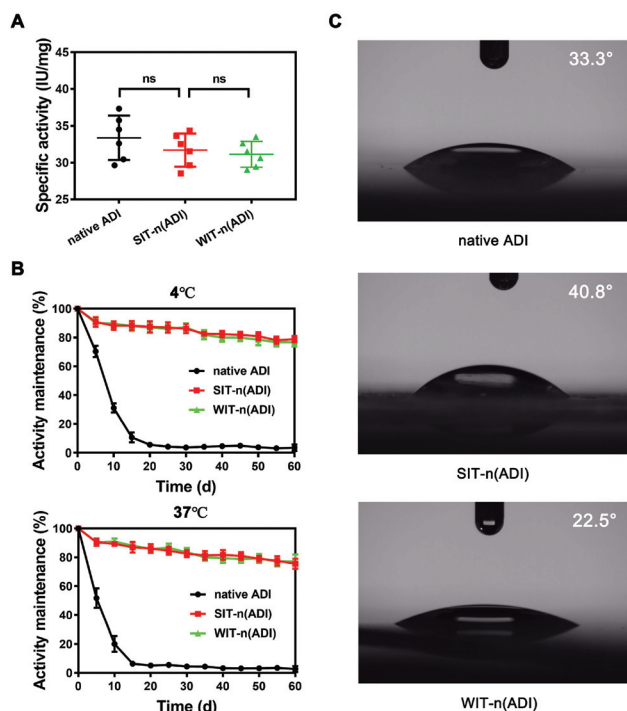
3.2 Activity maintenance of WIT-n(ADI)

The activity maintenance of ADI during the preparation process was tested. SIT-n(ADI) and WIT-n(ADI) could both efficiently convert arginine into citrulline, and their specific activity had no significant difference to that of native ADI (Fig. 2A), indicating that the mild preparation conditions caused little damage to ADI. Compared with chemical PEGylation, therefore, encapsulation through physical interaction was more suitable for the modification of ADI. The encapsulation of ADI dramatically enhanced its stability, further proving the above conclusion. Native ADI, SIT-n(ADI), and WIT-n(ADI) were respectively incubated with mice serum (volume ratio was 1 : 1) and stored at 4 °C and 37 °C. As shown in Fig. 2B, the activity of native ADI was nearly all lost after 20 days of storage, while that of SIT-n(ADI) and WIT-n(ADI) were

~80% of their initial activities even after 60 days, implying their *in vivo* application potential. Furthermore, the water contact angle experiments proved that the outer shell of WIT-n(ADI) was composed of the high content of PC, and therefore, it was much more hydrophilic than SIT-n(ADI) with the PAAM shell (Fig. 2C). The hydrophilic surface of WIT-n(ADI) could weaken the interaction between WIT-n(ADI) and cells, potentially avoiding the uptake of cells.

3.3 Cellular uptake of WIT-n(ADI)

To evaluate the cellular uptake of WIT-n(ADI), we incubated rhodamine B-labeled native ADI, SIT-n(ADI), and WIT-n(ADI) with HUVEC cells, H22 cells, and RAW 264.7 cells for 24 h. Fluorescence microscopy was used to track their localization. As shown in the right part of Fig. S3A,† native ADI was rarely taken up by HUVEC cells and H22 cells, while RAW 264.7 cells were capable of taking up a certain amount of native ADI. The encapsulation of ADI by PAAM-based polymeric shells changed the interaction between ADI and cells, resulting in the uptake of SIT-n(ADI) by HUVEC cells, H22 cells, and RAW 264.7 cells. On the contrary, PMPC-based polymeric shells

Fig. 2 Activity maintenance of WIT-n(ADI). (A) The specific activity measurement of native ADI, SIT-n(ADI), and WIT-n(ADI). The significance level is shown as $^{ns}p > 0.05$. (B) After incubation with mouse serum (volume ratio was $1:1$), native ADI, SIT-n(ADI), and WIT-n(ADI) were respectively stored at 4 °C and 37 °C, and their activities were tested for 60 days. (C) The water contact angle of films respectively formed by native ADI, SIT-n(ADI), and WIT-n(ADI).

could efficiently avoid the cellular uptake of WIT-n(ADI). The physicochemical property differences between MPC and AAM, which had been explained in our previous research,[23] caused the above-mentioned results. Furthermore, to exclude the effect of fluorescent dyes and further confirm the above observation, samples were also labeled with FITC and incubated with cells. The cellular uptake of FITC-labeled samples was consistent with that of rhodamine B-labeled samples (Fig. S3A,† left part). The cellular uptake efficiency quantified by flow cytometry further proved the above conclusions (Fig. S3B†). The cellular uptake efficiency of native ADI, SIT-n(ADI), and WIT-n(ADI) by HUVEC cells was respectively 2.20%, 13.93%, and 4.32%, while that of native ADI, SIT-n(ADI), and WIT-n(ADI) by H22 cells was respectively 15.52%, 66.54%, and 13.19%. RAW 264.7 cells had a more exceptional phagocytic ability, but they were still hard to take up WIT-n(ADI). The cellular uptake efficiency of WIT-n(ADI) by RAW 264.7 cells was 6.74%, while that of native ADI and SIT-n(ADI) was respectively 34.72% and 77.85%. These results indicated that WIT-n(ADI) could efficiently avoid the uptake of cells, even macrophages with strong phagocytic ability, potentially possessing the capacity of selective extracellular arginine deprivation.

PC-containing nanocarriers have been widely used for drug delivery. However, the influence of PC on the cellular uptake efficiency of these nanocarriers is often contradictory. On the one hand, it has been proved that nanoparticles with PC as the surface show the high efficiency of cellular uptake.[30,31] On the other hand, PC-coated nanoparticles could efficiently avoid the phagocytosis of macrophages, prolonging their circulation time.[24,32] In our own opinion, the surface content of PC has significant effects on the interaction between nanoparticles and cells. At low PC content, the surface of PC-functionalized nanoparticles may have defects such as hydrophobic micro-domain, and PC could enhance the interaction between these defects and cells because of its similar structure to the cell membrane.[33] The PC functionalization even results in the fusion of nanoparticles with cell membranes.[34] At high PC content, however, the non-defective surface of nanoparticles could reduce their cellular interaction avoiding cellular uptake. Specific to nanocapsules, when the PC surface filling ratio is higher than 58.3%, they could efficiently weaken the cellular interaction. When we adjust the PC surface filling ratio to 80%, the cellular uptake efficiency of WIT-n(ADI) is much lower than that of SIT-n(ADI). Moreover, the structure difference of PC-functionalized nanoparticles may affect their cellular interaction. For example, PC-modified micelles formed by block copolymers of different lengths show different cellular uptake efficiencies.[35]

To further verify that the cellular non-uptake of WIT-n(ADI) was due to its extremely weak cellular interaction, we tested the influence of cell wash on the cellular uptake of WIT-n(ADI). As shown in Fig. 3A, the fluorescence signals (green) of SIT-n(ADI) and WIT-n(ADI) were both detected in the cells that were directly observed without PBS washing. However, when the cells were washed twice with PBS, the fluorescence signal of WIT-n(ADI) disappeared. The results implied that WIT-n(ADI) had extremely weak interaction with cells because the simple wash process could affect the interaction between WIT-n(ADI) and cells. On the contrary, the interaction between SIT-n(ADI) and cells was not significantly affected by the cell wash process since the fluorescence signal of SIT-n(ADI) in the cells washed twice with PBS was still evident. The quantitative flow cytometry analysis showed that the cellular uptake efficiency of WIT-n(ADI) by unwashed HUVEC cells, H22 cell, and RAW 264.7 cells was respectively 18.26%, 28.13%, and 34.65% (Fig. 3B). In contrast, the cellular uptake efficiency of WIT-n(ADI) by PBS-washed HUVEC cells, H22 cell, and RAW 264.7 cells was 0.77%, 0.94%, and 1.29%, respectively. These results indicated that WIT-n(ADI) had extremely weak interaction with cells. It had been proved that the cellular uptake of nanoparticles was a process of energy consumption, and the cells would consume more energy to take up nanoparticles with weak cellular interaction than those with strong cellular interaction.[36] Therefore, the extremely weak cellular interaction of WIT-n(ADI) could result in too high energy consumption for cells to endocytose WIT-n(ADI).

It should be noted that WIT-n(ADI) has weak interactions with HUVEC cells, but it may not affect the accumulation of WIT-n(ADI) at the tumor site. It has been proved that nanocarriers can accumulate at the tumor site through the leaky vasculature of the tumor (the EPR effect). In addition, even if
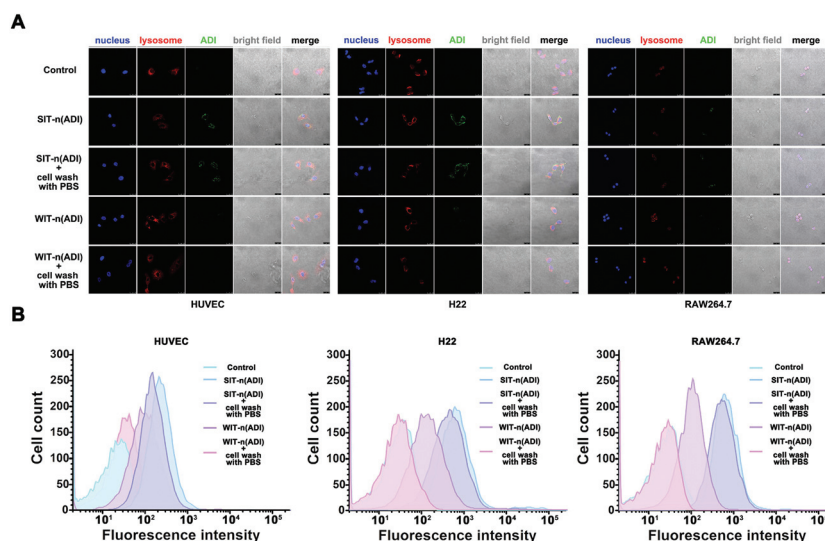
Fig. 3 Influence of cell wash on the cellular uptake of WIT-n(ADI). (A) Fluorescence microscopic images of HUVEC cells, H22 cells, and RAW 264.7 cells that were or were not washed with PBS after 4 h of incubation with SIT-n(ADI) and WIT-n(ADI). The bar was 20 μm. (B) Cellular uptake efficiency of SIT-n(ADI) and WIT-n(ADI) by cells that were or were not washed with PBS was assessed by flow cytometry.

WIT-n(ADI) cannot accumulate at the tumor site, they can consume arginine in the blood circulation to indirectly reduce the arginine content in the tumor tissues. Therefore, the extremely weak cellular interaction of WIT-n(ADI) would not affect its tumor therapeutic effects.

3.4 Cell viability and the intracellular ratio of citrulline to arginine

The cell viabilities of HUVEC cells, H22 cells, and RAW 264.7 cells were respectively tested. Fig. 4A shows the cell viability of HUVEC cells exposed to different concentrations of samples. At low concentrations (<30 ng mL^{-1}), native ADI, SIT-n(ADI), and WIT-n(ADI) had no discernible influence on HUVEC. When further increase in the concentrations of the samples, however, the cell viability of HUVEC cells treated with SIT-n (ADI) was decreased. At 100 ng mL^{-1}, the cell viability of HUVEC cells was ~65%. The cytotoxicity was related to the intracellular ratio of citrulline to arginine, which was gradually increased in HUVEC cells with the increase in SIT-n(ADI) concentrations. On the contrary, native ADI and WIT-n(ADI) could not be taken up by HUVEC cells and did not enhance the intracellular ratio of citrulline to arginine, possessing low cytotoxicity. Different from HUVEC cells, H22 cells did not express ASS1 and could not convert intracellular citrulline to arginine. Hence, either deprivation of extracellular arginine or deprivation of intracellular arginine by native ADI, SIT-n(ADI), and WIT-n(ADI) could efficiently improve the intracellular ratio of citrulline to arginine and suppress H22 cells (Fig. 4B). RAW 264.7 cells took up native ADI and SIT-n(ADI), resulting in their increased intracellular ratio of citrulline to arginine, and they had low cell viability in high concentrations of native ADI and SIT-n(ADI) (Fig. 4C). Due to the extremely limited WIT-n(ADI) in RAW 264.7 cells, the intracellular ratio of citrulline to
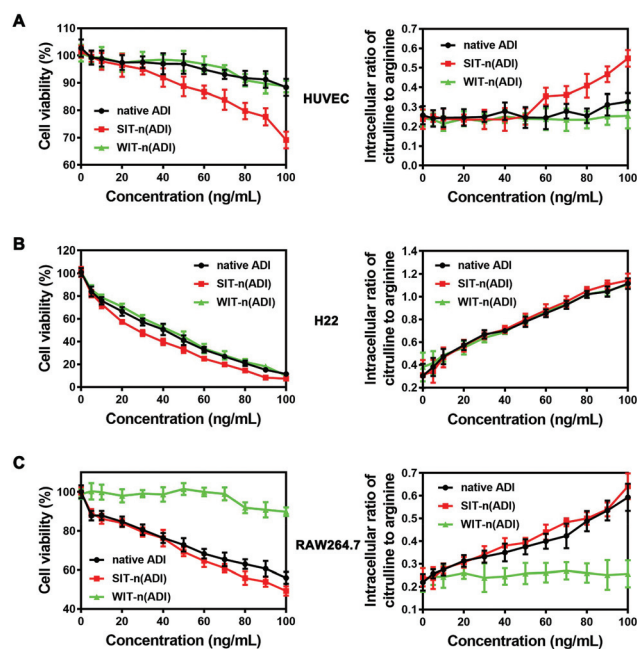
Fig. 4 Cell viability and the intracellular ratio of citrulline to arginine. (A) Left: The cell viability of HUVEC cells exposed to different concentrations of native ADI, SIT-n(ADI), and WIT-n(ADI). Right: The ratio of citrulline to arginine in HUVEC cells incubated with different concentrations of native ADI, SIT-n(ADI), and WIT-n(ADI). (B) Left: The cell viability of H22 cells exposed to different concentrations of native ADI, SIT-n(ADI), and WIT-n(ADI). Right: The ratio of citrulline to arginine in H22 cells incubated with different concentrations of native ADI, SIT-n(ADI), and WIT-n(ADI). (C) Left: The cell viability of RAW 264.7 cells exposed to different concentrations of native ADI, SIT-n(ADI), and WIT-n(ADI). Right: The ratio of citrulline to arginine in RAW 264.7 cells incubated with different concentrations of native ADI, SIT-n(ADI), and WIT-n(ADI).

arginine was always stable at the normal level, and the viability of RAW 264.7 cells was consistently high. These results indicated that WIT-n(ADI) could efficiently increase the ratio of citrulline to arginine in cells that did not express ASS1. In contrast, they did not affect normal ASS1-expressed cells because of their cellular non-uptake property, potentially facilitating the clinical translation of metabolic enzyme-based amino acid deprivation therapy.

ADI has previously shown anti-angiogenic properties due to its inhibitory effect on endothelial cell growth.[37] Still, our results indicated that native ADI and WIT-n(ADI) did not seriously affect the cell viability of HUVEC cells. This may be because the apoptosis of endothelial cells could be induced only at high concentrations of ADI.[37] At a low level of ADI, the extracellular deprivation of arginine does not disrupt the intracellular amino acid balance because normal cells can take advantage of extracellular citrulline to generate intracellular arginine. In contrast, ASS1-deficient cells such as H22 cells cannot make use of extracellular citrulline, and low concentrations of ADI would efficiently deprive both the extracellular arginine and the intracellular arginine inducing the apoptosis of these cells.

It should be noted that once ADI enters the cells, the intracellular amino acid balance is readily disrupted even at low concentrations. This is because SIT-n(ADI) shows higher cytotoxicity to HUVEC cells than native ADI and WIT-n(ADI) at the same concentration. Therefore, it is essential to maintain the cellular non-uptake property of ADI for inhibiting the proliferation of ASS1-deficient cells and avoiding the cytotoxicity to normal cells.

3.5 *In vivo* activity and immune response of WIT-n(ADI)

The *in vivo* activity of native ADI, SIT-n(ADI), and WIT-n(ADI) was tested. The cellular non-uptake property of WIT-n(ADI) dramatically enhanced its blood circulation time. As shown in Fig. 5A, the half-life time of native ADI and SIT-n(ADI) was respectively ∼2 h and ∼8 h, while that of WIT-n(ADI) was ∼90 h, and even after 240 h, ∼25% of WIT-n(ADI) could still be present in the blood. Fig. 5B shows the ratio of citrulline to arginine in plasma. The initial ratio of citrulline to arginine in plasma was 0.55 ± 0.17, while it was instantly increased to several hundred after systemic administration of native ADI, SIT-n(ADI), and WIT-n(ADI). In the native ADI group and SIT-n (ADI) group, however, the ratio of citrulline to arginine in plasma was quickly decreased. After 96 h, the ratio in the native ADI group returned to normal. The performance of SIT-n(ADI) was slightly better, but its function only lasted 144 h. The super-long blood circulation of WIT-n(ADI) realized its
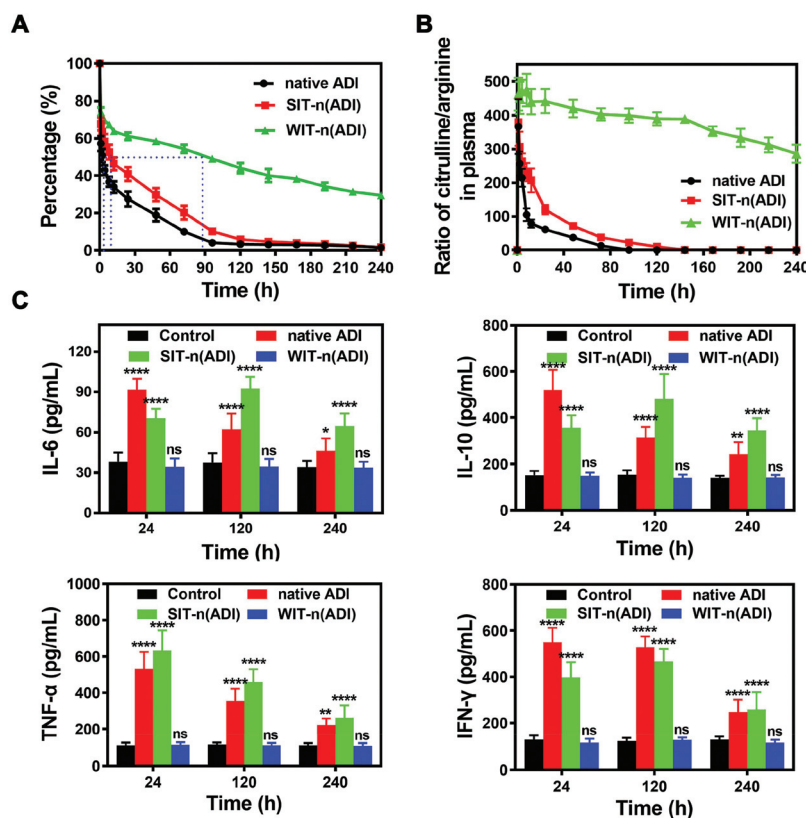
Fig. 5 *In vivo* activity measurement. (A) Circulation time of native ADI, SIT-n(ADI), and WIT-n(ADI). ADI was labeled with rhodamine B. (B) Ratio of citrulline to arginine in the plasma of mice, which were injected with native ADI, SIT-n(ADI), and WIT-n(ADI). The ADI equivalent was ∼1 mg. (C) Cytokine levels in mouse blood after different times of sample administration. Significantly different from the control group, $^{ns}p > 0.05$, $*p < 0.05$, $**p < 0.01$, and $****p < 0.001$.

sustained catalysis of arginine in plasma. After 240 h, the ratio in the WIT-n(ADI) group was still higher than 280. Furthermore, the ratio of citrulline to arginine in the tumor tissue was also tested. As shown in Fig. S4,† SIT-n(ADI) and WIT-n(ADI) could both increase the ratio of citrulline to arginine in tumor tissues, and WIT-n(ADI) showed sustained catalysis of arginine for several days. These results indicated that the steady high ratio of citrulline to arginine in the plasma caused by WIT-n(ADI) could induce the high intracellular ratio of citrulline to arginine in ASS1-deficient tumor cells, potentially suppressing these tumors. We further evaluated the immunogenicity of *in vivo* use of WIT-n(ADI) by measuring the inflammatory cytokine secretion from the mice treated with WIT-n(ADI) (Fig. 5C). Native ADI and SIT-n(ADI) could stimulate the abundant secretion of inflammatory cytokines, and the levels of inflammatory cytokines were still much higher than the normal values ever after 10 days of sample administration. On the contrary, no significant change in inflammatory cytokine secretion was observed in the blood of mice treated with WIT-n(ADI), indicating its low immunogenicity.

3.6 *In vivo* cellular non-uptake property of WIT-n(ADI)

To realize the selective extracellular arginine deprivation, WIT-n(ADI) should possess the *in vivo* cellular non-uptake property. We deduced that cardiac perfusion with PBS could eliminate samples in mouse blood, facilitating to confirm the *in vivo* location of native ADI, SIT-n(ADI), and WIT-n(ADI). We labeled samples with a fluorescence probe Cy5.5 that was then injected intravenously into normal nude mice. After 24 h of administration, the *in vivo* biodistribution of Cy5.5-labeled samples was monitored using a noninvasive near-infrared fluorescence (NIRF) optical imaging technique. The excitation and emission wavelengths were set at 675 and 720 nm, respectively (Fig. 6A). Fluorescence signals of native ADI, SIT-n(ADI), and WIT-n(ADI) were mainly observed in the abdomen of mice. *Ex vivo*

NIRF optical images of organs harvested from these mice further showed that the majority of samples accumulated in the liver (Fig. 6B, left part). However, after cardiac perfusion, the fluorescence signal in the liver was all weakened, and it was undetectable in the liver of mice injected with WIT-n(ADI) (Fig. 6B, right part). The quantitative region-of-interest analysis revealed that the fluorescence signal intensity in the liver of mice injected with WIT-n(ADI) after cardiac perfusion decreased ~20-fold (Fig. S5†). The liver is one of the main organs that contain a lot of blood in animals. The fluorescence signal of WIT-n(ADI) in the liver declined rapidly after cardiac perfusion, implying its storage in blood. The fluorescence signal of WIT-n(ADI) in other organs, in particular the spleen, which also contains a lot of blood, was almost undetectable after cardiac perfusion, further proving the above conclusion. In contrast, the fluorescence signals of native ADI and SIT-n(ADI) in the liver after cardiac perfusion were decreased, but their intensities were still high. The possible cause of this phenomenon was the cellular uptake of these samples in the liver. The fluorescence signal of native ADI and SIT-n(ADI) in the liver section of mice treated with cardiac perfusion was much higher than that of WIT-n(ADI), further indicating that WIT-n(ADI) had cellular non-uptake property and was always in the blood (Fig. S6†).

In previous research studies, the accumulation of samples in organs, such as tumors, livers, and brains, is often tested. In related tests, actually, how much samples accumulated in the parenchyma of organs is the focus. Here, we proved that the fluorescence signal intensities of WIT-n(ADI) in organs were dramatically decreased after cardiac perfusion with PBS. This result indicates that the samples in the blood could affect the test of sample accumulation in organs. To measure the content of samples accumulated in the parenchyma of organs, we should eliminate the influence of the samples located in the blood of organs. To the best of our knowledge, this issue is often ignored in related research.
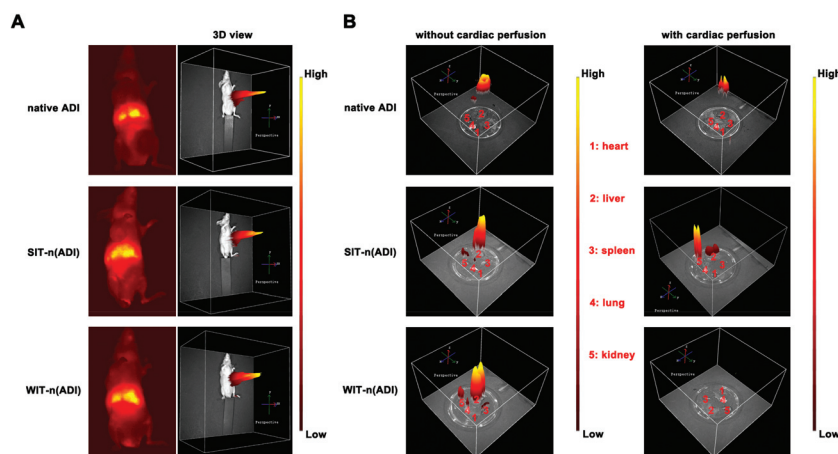

Fig. 6 *In vivo* cellular non-uptake property of WIT-n(ADI). (A) After 24 h of intravenous injection, noninvasive NIRF imaging of Cy5.5-labeled native ADI, SIT-n(ADI), and WIT-n(ADI) in nude mice. (B) Representative *ex vivo* NIRF optical images of organs harvested from mice treated with cardiac perfusion after 24 h of intravenous injection of samples.

3.7 Tumor suppression by a single injection of WIT-n(ADI)

The tumor inhibition effects of WIT-n(ADI) on H22-bearing mice were investigated. After 4 days of tumor inoculation, tumor-bearing mice were injected intravenously with native ADI, SIT-n(ADI), and WIT-n(ADI) only once. The body weights of mice in different groups were monitored (Fig. S7†), and they had no significant difference during the treatment process. The body weights of mice in the native ADI group and SIT-n (ADI) group showed a temporary decline potentially caused by

their side effects. To examine the kinetics of tumor growth, we monitored the tumor volume using a caliper every 3 days and calculated as $[(\text{length} \times \text{width}^2)/2]$. The tumor volumes of mice treated with PBS increased rapidly within 13 d (Fig. 7A). Native ADI could inhibit tumor growth to some extent, but the tumor volume of mice in the native ADI group was similar to that in the control group after 22 d. SIT-n(ADI) showed a strong ability to inhibit tumor growth because the tumor volume of mice in the SIT-n(ADI) group was much smaller than that in the native ADI group in the initial 13 d. However, the tumor volume
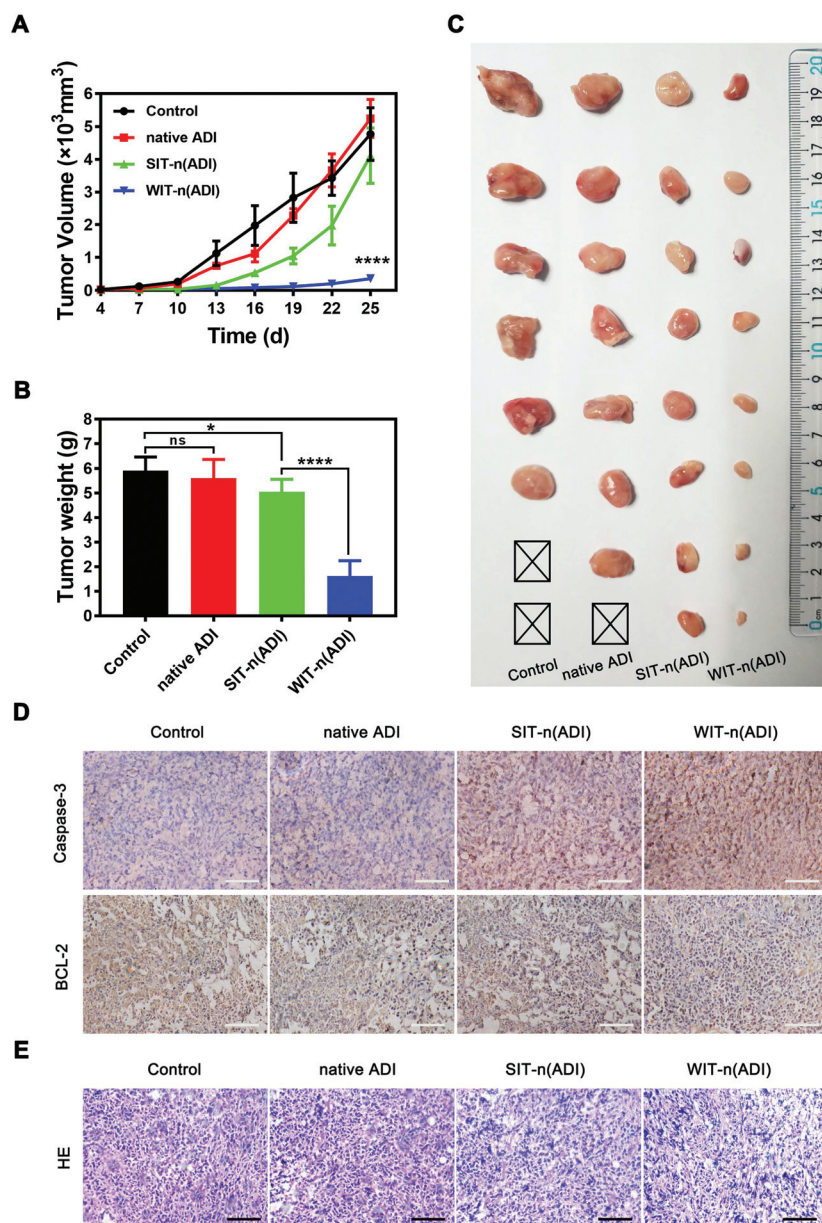
Fig. 7 Tumor suppression. (A) Growth evaluation of H22 subcutaneous tumor in Kunming mice after sample administration. Tumor volume was examined every 3 days for 21 consecutive days. (B) Average mass of collected tumor tissues. (C) H22 tumor tissues obtained from euthanized mice after 21 days of sample administration and a rectangle represented the dead mice. (D) Immunohistochemistry analyses of the expression of caspase-3 and Bcl-2 in each group. Nuclei were stained blue, and the proteins were stained brown. The bar was 200 μm. (E) H&E staining and significance levels are shown as $^{ns}p > 0.05$, $^*p < 0.05$, and $^{****}p < 0.001$.

increased quickly after 13 d because of the invalidation of SIT-n(ADI). In contrast, WIT-n(ADI) possessed the ability of sustained tumor suppression. The tumor volume of mice in the WIT-n(ADI) group was much smaller than that in other groups after 25 d. The weights of tumor harvested from the mice in the group of PBS, native ADI, SIT-n(ADI), and WIT-n(ADI) on day 25 were ∼5.92 g, ∼5.61 g, ∼5.04, and ∼1.62 g, respectively (Fig. 7B). Fig. 7C showed tumor tissues obtained from euthanized mice on day 25, and a rectangle represented the dead mice. Tumor tissues of mice in the WIT-n(ADI) group had a much smaller size than that in other groups, indicating the excellent tumor inhibition efficiency of WIT-n(ADI). It had been proved that arginine deprivation could trigger the apoptosis of the tumor cells.[38] Here, we examined the expression levels of caspase-3 and Bcl-2 in tumor tissues harvested from these mice by using immunohistochemistry analyses (Fig. 7D). WIT-n(ADI) could dramatically suppress the tumor growth and up-regulate the apoptosis of H22 cells by decreasing Bcl-2 expression and increasing caspase-3 expression. The result was also confirmed by the direct observation of the slices stained with H&E (Fig. 7E). These results indicated the feasibility of selectively depriving extracellular arginine using WIT-n(ADI) for the treatment of ASS1-deficient tumors.

3.8 Biological safety of WIT-n(ADI)

To verify whether selective extracellular arginine deprivation avoided the side effects, we examined the histological sections of organs (heart, liver, spleen, lung, and kidney) stained with

H&E (Fig. 8A). It could be observed that native ADI and SIT-n(ADI) did not cause apparent damage to most organs except for the liver. In the native ADI group and the SIT-n(ADI) group, the morphologies of the hepatic sinusoid and the hepatic lobule were irregular, indicating their hepatotoxicity. This conclusion was further proved by the measurement of the liver function index (Fig. 8B). Tests of the serum level of total protein (TP), alanine aminotransferase (ALT), aspartate aminotransferase (AST), and alkaline phosphatase (ALP) showed that the liver function of mice in the native ADI group and the SIT-n(ADI) group was impaired, while that in the WIT-n(ADI) group was normal. These results demonstrated the high biosafety of selective extracellular arginine deprivation.

To date, PEGylated ADI is the most successful functionalized ADI, and it has been used in clinical trials. As an example, ADI-PEG20 has been a novel targeted therapy for both hepatocellular carcinoma and malignant melanoma. However, the toxicity of PEGylated ADI cannot be ignored. For example, in phase I/II trial of ADI-PEG20 for the treatment of unresectable hepatocellular carcinoma, 12 patients (43%) had grade 3 toxicity, and 3 patients (8.5%) had grade 4 toxicity.[39] The most common acute toxicity was related to liver function, and this phenomenon may be due to the hepatocyte phagocytosis of ADI-PEG20. Therefore, compared with PEGylated ADI, WIT-n(ADI) possessing the cellular non-uptake property has more significant potential for clinical translation.

In previous drug delivery research studies, the focus of the researchers is mainly on how to improve the weakness of
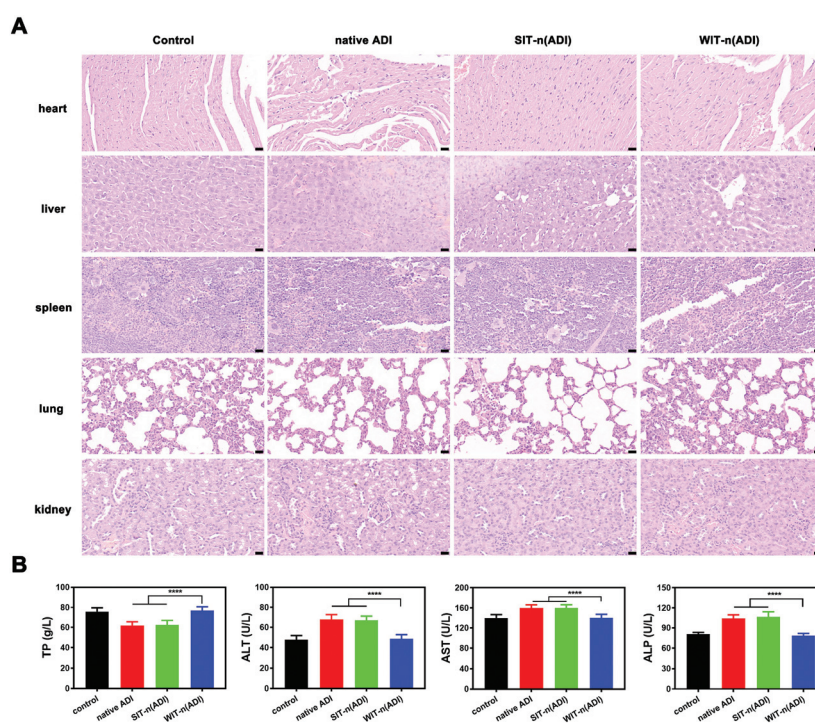
Fig. 8 Biological safety. (A) Histological sections of organs stained with H&E, and the bar was 20 μm. (B) Serum levels of total protein (TP), alanine aminotransferase (ALT), aspartate aminotransferase (AST), and alkaline phosphatase (ALP) in mouse blood of different groups. The significance level is shown as ****$p < 0.001$.

drugs, while how to maintain the advantages of drugs is often ignored. Actually, the functionalization of drugs, such as constructing nanomedicines, may weaken its benefits. For example, hydrophobic chemotherapeutics could directly diffuse into cells, but their active diffusion capacity is potentially deprived when they are exploited as nanomedicines. To enter into the cytoplasm, they have to be released from the nanocarriers and escape from endosomes, and the intracellular enrichment efficiency would decrease. On the contrary, drugs that do not need to get into cells, such as certain kinds of proteins, may be delivered into cells when they are functionalized, causing undesirable side effects. In our own opinions, therefore, the functionalization of drugs should not only improve its weakness but also maintain its advantages.

4. Conclusion

A kind of nanocapsule with extremely weak cellular interaction was exploited. These nanocapsules can load ADI to dramatically increase its circulation time and reduce its immunogenicity, efficiently improving the weakness of native ADI. Furthermore, the nanocapsules do not change the cellular non-uptake property of ADI, selectively depriving extracellular arginine and avoiding the destruction of the intracellular amino acid balance and the resulting cell damage. This new strategy first realizes the selective extracellular arginine deprivation for the treatment of ASS1-deficient tumors, potentially promoting the clinical translation of metabolizing enzyme-based amino acid deprivation therapy. Besides, the research reminds us that the functionalization of drugs should not only improve its weakness but also maintain its advantages.

Conflicts of interest

The authors have declared that no competing interest exists.

Acknowledgements

References

1 B. A. Teicher, W. M. Linehan and L. J. Helman, *Clin. Cancer Res.*, 2012, **18**, 5537–5545.

2 M. K. L. Fung and G. C. Chan, *J. Hematol. Oncol.*, 2017, **10**, 144.

3 C. R. Morris, J. Hamilton-Reeves, R. G. Martindale, M. Sarav and J. B. Ochoa Gautier, *Nutr. Clin. Pract.*, 2017, **32**, 30S–47S.

4 B. Delage, D. A. Fennell, L. Nicholson, I. McNeish, N. R. Lemoine, T. Crook and P. W. Szlosarek, *Int. J. Cancer*, 2010, **126**, 2762–2772.

5 L. Feun, M. You, C. J. Wu, M. T. Kuo, M. Wangpaichitr, S. Spector and N. Savaraj, *Curr. Pharm. Des.*, 2008, **14**, 1049–1057.

6 M. M. Phillips, M. T. Sheaff and P. W. Szlosarek, *Cancer Res. Treat.*, 2013, **45**, 251–262.

7 J. M. Bratt, A. A. Zeki, J. A. Last and N. J. Kenyon, *J. Biomed. Res.*, 2011, **25**, 299–308.

8 S. Dabir, P. Dabir and B. Somvanshi, *Int. J. Biol. Sci.*, 2005, **1**, 114–122.

9 C. Alexandrou, S. S. Al-Aqbi, J. A. Higgins, W. Boyle, A. Karmokar, C. Andreadi, J. L. Luo, D. A. Moore, M. Viskaduraki, M. Blades, G. I. Murray, L. M. Howells, A. Thomas, K. Brown, P. N. Cheng and A. Rufini, *Sci. Rep.*, 2018, **8**, 12096.

10 F. W. Holtsberg, C. M. Ensor, M. R. Steiner, J. S. Bomalaski and M. A. Clark, *J. Controlled Release*, 2002, **80**, 259–271.

11 J. J. Harding, R. K. Do, I. E. Dika, E. Hollywood, K. Uhlitskykh, E. Valentino, P. Wan, C. Hamilton, X. Feng, A. Johnston, J. Bomalaski, C. F. Li, E. M. O'Reilly and G. K. Abou-Alfa, *Cancer Chemother. Pharmacol.*, 2018, **82**, 429–440.

12 G. K. Abou-Alfa, S. Qin, B. Y. Ryoo, S. N. Lu, C. J. Yen, Y. H. Feng, H. Y. Lim, F. Izzo, M. Colombo, D. Sarker, L. Bolondi, G. Vaccaro, W. P. Harris, Z. Chen, R. A. Hubner, T. Meyer, W. Sun, J. J. Harding, E. M. Hollywood, J. Ma, P. J. Wan, M. Ly, J. Bomalaski, A. Johnston, C. C. Lin, Y. Chao and L. T. Chen, *Ann. Oncol.*, 2018, **29**, 1402–1408.

13 B. Li, Z. Yuan, Y. He, H. C. Hung and S. Jiang, *Nano Lett.*, 2020, **20**, 4693–4699.

14 T. Zeng, Y. Zhang, Q. Yan, Z. Huang, L. Zhang, X. Yi, J. Chen, G. He and Y. Yin, *Carbohydr. Polym.*, 2017, **162**, 35–41.

15 F. L. Wu, T. H. Yeh, Y. L. Chen, Y. C. Chiu, J. C. Cheng, M. F. Wei and L. J. Shen, *Mol. Pharm.*, 2014, **11**, 2777–2786.

16 T. H. Yeh, Y. R. Chen, S. Y. Chen, W. C. Shen, D. K. Ann, J. L. Zaro and L. J. Shen, *Mol. Pharm.*, 2016, **13**, 262–271.

17 Q. Shao and S. Jiang, *Adv. Mater.*, 2015, **27**, 15–26.

18 B. Li, Z. Yuan, H. C. Hung, J. Ma, P. Jain, C. Tsao, J. Xie, P. Zhang, X. Lin, K. Wu and S. Jiang, *Angew. Chem., Int. Ed.*, 2018, **57**, 13873–13876.

19 B. Li, J. Xie, Z. Yuan, P. Jain, X. Lin, K. Wu and S. Jiang, *Angew. Chem., Int. Ed.*, 2018, **57**, 4527–4531.

20 H. Qi, H. Yang, X. Li, X. Sun, J. Zhao, X. Hou, Z. Li, X. Yuan, Z. Cui and X. Yang, *Biomater. Sci.*, 2019, **7**, 1675–1685.

21 L. Yang, D. Han, Q. Zhan, X. Li, P. Shan, Y. Hu, H. Ding, Y. Wang, L. Zhang, Y. Zhang, S. Xue, J. Zhao, X. Hou, Y. Wang, P. Li, X. Yuan and H. Qi, *Theranostics*, 2019, **9**, 7680–7696.

22 J. Ge, D. Lu, J. Wang, M. Yan, Y. Lu and Z. Liu, *J. Phys. Chem. B*, 2008, **112**, 14319–14324.

23 S. Li, L. Chen, K. Huang, N. Chen, Q. Zhan, K. Yi, H. Qi, C. Liu, Y. Tan, X. Hou, Y. Lu, J. Zhao, X. Yuan and C. Kang, *Adv. Funct. Mater.*, 2019, **29**, 1903296.

24 S. Liang, Y. Liu, X. Jin, G. Liu, J. Wen, L. Zhang, J. Li, X. Yuan, I. S. Y. Chen, W. Chen, H. Wang, L. Shi, X. Zhu and Y. Lu, *Nano Res.*, 2016, **9**, 1022–1031.

25 M. J. Tamas, S. K. Sharma, S. Ibstedt, T. Jacobson and P. Christen, *Biomolecules*, 2014, **4**, 252–267.

26 K. Ishihara, M. Mu, T. Konno, Y. Inoue and K. Fukazawa, *J. Biomater. Sci., Polym. Ed.*, 2017, **28**, 884–899.

27 E. Blanco, H. Shen and M. Ferrari, *Nat. Biotechnol.*, 2015, **33**, 941–951.

28 O. Wiarachai, T. Vilaivan, Y. Iwasaki and V. P. Hoven, *Langmuir*, 2016, **32**, 1184–1194.

29 K. G. Uranta, S. Rezaei-Gomari, P. Russell and F. Hamad, *Energies*, 2018, **11**, 2201.

30 M. Ukawa, H. Akita, T. Masuda, Y. Hayashi, T. Konno, K. Ishihara and H. Harashima, *Biomaterials*, 2010, **31**, 6355–6362.

31 S. Tu, Y. W. Chen, Y. B. Qiu, K. Zhu and X. L. Luo, *Macromol. Biosci.*, 2011, **11**, 1416–1425.

32 J. Zhao, Y. D. Chai, J. Zhang, P. F. Huang, K. Nakashima and Y. K. Gong, *Acta Biomater.*, 2015, **16**, 94–102.

33 Y. Iwasaki and K. Ishihara, *Sci. Technol. Adv. Mater.*, 2012, **13**, 064101.

34 W. Zhou, J. Shao, Q. Jin, Q. Wei, J. Tang and J. Ji, *Chem. Commun.*, 2010, **46**, 1479–1481.

35 Y. Cai, S. Li, M. Cai, Y. Chen and X. Luo, *New J. Chem.*, 2017, **41**, 11828–11838.

36 S. Behzadi, V. Serpooshan, W. Tao, M. A. Hamaly, M. Y. Alkawareek, E. C. Dreaden, D. Brown, A. M. Alkilany, O. C. Farokhzad and M. Mahmoudi, *Chem. Soc. Rev.*, 2017, **46**, 4218–4244.

37 K. Beloussow, L. Wang, J. Wu, D. Ann and W. C. Shen, *Cancer Lett.*, 2002, **183**, 155–162.

38 G. Y. Shuvayeva, Y. P. Bobak, O. I. Vovk, L. A. Kunz-Schughart, M. T. Fletcher and O. V. Stasyk, *Cell Biol. Int.*, 2020, 1–10.

39 P. A. Ott, R. D. Carvajal, N. Pandit-Taskar, A. A. Jungbluth, E. W. Hoffman, B. W. Wu, J. S. Bomalaski, R. Venhaus, L. Pan, L. J. Old, A. C. Pavlick and J. D. Wolchok, *Invest. New Drugs*, 2013, **31**, 425–434.